Characterization of Rod-like High-purity Fluorapatite Nanopowders Obtained by Sol-gel Method

N. Sasani[1], H. Khadivi Ayask[1], S. M. Zebarjad[1], J. Vahdati Khaki[1]

Abstract

In this research, high purity fluorapatite (FA) with rod-like and spherical-like morphology was synthesized via sol-gel method. Triethyl phosphate $[(C_2H_5)_3PO_4]$ and calcium nitrate $[Ca (NO_3)_2]$ were used as precursors under an ethanol-water based solution for FA production. Controlled amounts of ammonium fluoride (NH_4F) were incorporated for the preparation of the FA sol-gels. FA gels were prepared by mixing of P, F and Ca sols and subsequently drying and calcination of gels. In this work, the effects of some sol-gel parameters have investigated on gelation time of FA. Chemical characterization of FA powders was done by XRD and FTIR analyses. Crystallite samples were calculated using Scherer method. Morphology of FA powders was investigated with TEM and SEM images. The results revealed that increasing the time of hydrolysis of phosphate sols significantly decreased the gelation time of FA sols. Also, mixing temperature of P and Ca sols affects the gelation time of samples and increasing pH decreases the gelation time of FA sols. Morphological and chemical characterization of samples showed that the FA powders have high purity and rod-like and spherical-like morphology.

Keywords: Fluorapatite; Sol-Gel; Rod-like; High-purity; Nanopowders

1. Introduction

Hydroxyapatite [HA, $Ca_{10} (PO_4)_6(OH)_2$] ceramics have long been used as materials for the rehabilitation or replacement of skeletal tissues in orthopedics and dentistry due to their chemical and biological similarity to human hard tissues (Kim et al., 2004; Ebrahimi-kahrizsangi et al., 2010). However, pure HA suffers from relatively high dissolution rate in the biological environment, poor corrosion resistance in an acid environment and poor chemical stability in high-temperature (Fini et al., 2003: Chen & Miao, 2005).

Implant fixation to the host tissue is seriously hindered if the HA dissolution rate is too fast (Block et al., 1989). Substitution of F^- in HA structure plays one of the leading roles because of its influence on the physical and biological properties of HA (Nikcˇevic et al., 2004). Substitution of OH^- by F^- in HA causes an increase in chemical stability, a decrease in mineral solubility, and a promotion in bone cell proliferation (Ebrahimi-kahrizsangi et al., 2010). Moreover, fluoride ion can reduce the formation of caries in bacterially contaminated environments and promotes mineralization and crystallization of calcium phosphates in the formation of bone (Marie & Hott, 1986).

Recently, fluorine-substituted hydroxyl apatite has attracted much attention, and has increasingly been studied as a clinical restoration material. Over the past decades, various synthesis methods of FA have been reported, including precipitation (Rintoul et al., 2007), sol–gel (Cavalli et al., 2001), solid-state reaction (Fa´bia´na et al., 1998), mechanical alloying (Fathi & Mohammadi Zahrani, 2009), molten salt synthesis (Zhang & Zhu, 2006) and electrochemical deposition (Wang et al., 2009). The sol-gel technique offers many potential advantages in terms of chemical homogeneity, fine grain microstructure, low crystallization temperature, and mass producibility (Brendel et al., 1992). But there are few reports concerning the fabrication, characterization and optimization of the FA materials produced via the sol-gel route.

1- Department of Materials Science and Engineering, Engineering Faculty, Ferdowsi University of Mashhad, Mashhad, Iran.

Corresponding author: N. Sasani, Department of Materials Science and Engineering, Engineering Faculty, Ferdowsi University of Mashhad, Mashhad, Iran.
Email: na.sasani@stu.um.ac.ir

In the present research, the effects of some sol-gel parameters have been investigated on the synthesis of FA nanopowders. The effects of some sol-gel parameters were also investigated on gelation time of FA. XRD and FTIR analyses were used for chemical characterization of FA powders. Morphology of FA powders was investigated with TEM and SEM images. The UV–Vis absorption spectra of the FA samples were recorded to determine the optical band gap.

2. Experimental

Materials and concentrations used for the preparation of FA sol-gel are shown in Table 1. Controlled amounts of triethyl phosphate (TEP) ($[(C_2H_5)3PO_4]$, Merck) and ammonium fluoride (NH_4F, Merck) were first dissolved in ethanol and water and then the solution was stirred vigorously for various time and temperature. After hydrolysis process, phosphate sol was slowly added to a solution of calcium nitrate [Ca $(NO_3)_2$] (Merck) and allowed to mix for a further time and temperature until gelation of sol occurred.

Each composition ratio in the FA sol was adjusted to have [Ca]/ [P] = 1.67 and [P]/ [F] = 3 in order to produce the corresponding compositions of [$Ca_{10} (PO_4)6F_2$]. Ammonium hydroxide (NH_4OH, Merck) and nitric acid (HNO_3 Merck) was used as pH modifiers.

The gels have been dried at 80ºC in air atmosphere and then heat treated at 550 ºC for

Table 1. Materials used for FA sol preparation.

No.	Name	Composition	Conc. (M)
1	triethyl phosphate	$(C_2H_5O)_3PO_4$	1
2	calcium nitrate-tetra hydrate	$Ca(NO_3)_2 \cdot 4H_2O$	1.67
3	ammonium fluoride	NH_4F	0.33
4	ammonium hydroxide	NH_4OH	Various amounts
5	nitric acid	HNO_3	Various amounts
6	ethanol	C_2H_6O	3
7	water	H_2O	4

1 h. The phase and composition of the nanopowders were analyzed by means of x-ray diffraction XRD (X-ray diffractometer (Philips model PW1800 with Cu Kα radiation) and FTIR analyses (AVATAR-370-FTIR Thermonicolet). Crystallite size of powders was calculated from x-ray patterns using Xpert software and Scherer method. Morphology and shape of nanopowders were analysed with scanning electron microscopy (SEM) and transmission electron microscopy (TEM). TEM analysis of powders was done after 15 minutes ultrasonic in ethanol to collapse the agglomerated powders. The UV–Vis spectroscopy (LABOMET-4057UVvis) was used for determination of FA optical band gap.

3. Result and Discussion

3.1. Synthesis of FA

The FA sols were transformed to gels through solvent evaporation and then were heat treated. Figure 1 shows the XRD pattern of FA nanopowders heat treated at 550 ºC for 1h. Hydrolysis time and temperature of FA sols was set at 20h and 60 ºC respectively. NH_4OH was used to adjust the pH to about 11. It can be seen that pure FA was synthesised at these process conditions. Mean crystallite size of FA phase after heat treatment at 550 ºC was calculated by Scherer method to be about 70 nm.

Figure 2 shows functional groups of the FA powder. The FTIR spectra of fluorapatite indicates 575.21 and 603.51 cm−1 for the bending stretching of PO and 1039.56 cm−1 for vibration of the asymmetrical stretching of PO group. A broad peak at 2800–3600 cm−1

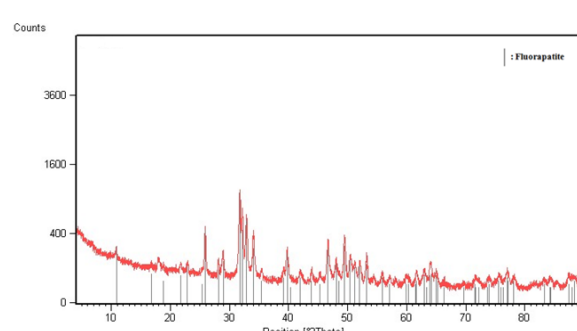**Fig. 1.** XRD pattern of pure FA powder synthesised at pH≈11, hydrolysis time = 20h and hydrolysis temperature = 60º C

could be related to the OH groups. The band at 3539.99 cm-1 corresponds to symmetric stretching vibration of hydroxyl ions. The absence of OH band at 630 cm-1, and the appearance of the band at 712.89 and 747.14 cm-1 correspond to the shifting of OH vibration. A small peak at 3642.37 cm−1 could be related to the OH—F bond, which proves that fluoride ion penetrates into the apatite network. The peak 1634.31 cm−1 relates to the water-bending mode (Brendel et al., 1992). The narrow peak at 1453.78 cm−1 can be attributed to CO_3^{2-} ion in fluorapatite network (Ebrahimi-kahrizsangi et al., 2010). The presence of this carbonated group improves the bioactivity of FA (Lafon et al., 2008; Sanosh et al., 2009). Also, the presence of the peak at 873.99 cm−1 can be related to carbonated group or hydrogen phosphate (HPO_4^{2-}) (Nikčevic et al., 2004). Substitution of different ions in the apatite structure reduces the symmetry in the FTIR spectrum. The FTIR and XRD spectrum of the FA powder reveals that the synthesized powder has high degree of purity.

UV-visible analysis was carried out in order to characterize the optical absorbance of the FA nanopowder. Figure 3 shows the absorption spectra and Tauc's plots (Yadav et al., 2010, Mehta et al., 2010) of pure FA nanopowders. The band gap of pure FA has not been studied previously. It is seen that an absorption edge located at about 310 nm occurs in case of FA particles. The band gap value of the FA particles was obtained by optical absorption measurements and plotting $(\alpha h\nu)^2$ versus photon energy ($h\nu$) (Fig. 3b)
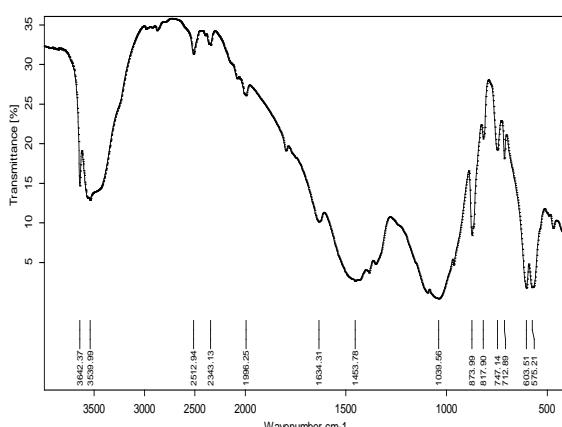
according to the following equation (Tauc's relation) (Yadav et al., 2010, Mehta et al., 2010):

$$(\alpha h\nu)^2 = A(h\nu - E_g)$$

where α is the absorption coefficient, A and E_g are constant and band gap of the particles, respectively. The band gaps of pure FA calculated was determined to be about 4.3 eV. Few studies have been conducted to evaluate the band gap of apatite materials including HA. In one paper, the band gap of HA was reported to be 3.95 eV by photoluminescence measurement (Aronov et al., 2007; Tsukada et al., 2011). It appears that FA exhibits photocatalytic activity in the near-ultraviolet region. The band gap of FA exceeded the range of Vis.

The clinical success of dental implants with apatite coating could be jeopardized by bacterial infection inducing mucositis or periimplantitis (Mombelli et al., 1987;
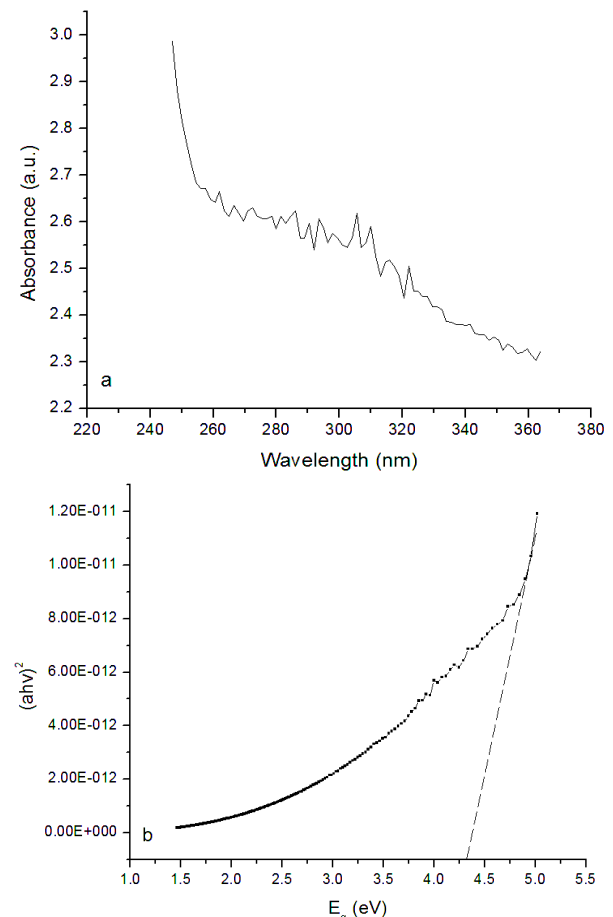
Fig. 3. (a) UV-Vis absorption spectra and (b) band gap calculation from Tauc's relation for FA.

Fig. 2. FTIR spectra of fluorapatite powders calcinated in 550°C for 1h.

Leonhardt et al., 1992; Lindhe et al., 1992; Jason Riley et al., 2005). Among Several methods for the cleaning of a failing implant surfaces, laser treatment seemed to be effective in terms of bacteria elimination (Jason Riley et al., 2005; Kreisler et al., 2002; Kreisler et al., 2003; Dortbudak et al., 2001). It has been reported that illumination with infra-red lasers is possible to damage the surface of the implant (Jason Riley et al., 2005; Kreisler et al., 2002). The second method is sensitizing the implant surface with an organic molecule that absorbs laser light and uses the energy to produce highly reactive chemical agents that attack the bacteria (Riley et al., 2005; Matysik et al., 2002). Previous researches indicate that polluting components including bacteria, viruses, NOx, ammonia and toxic chemical compounds are immediately absorbed by apatites (Kangwansupamonkon et al., 2009; Nonami et al., 1998). The UV spectrum has the range from 100 to 400 nm. The FA, with band gap of 4.3 eV, absorbs UV (used for sterilization of implant) and act as a photocatalyst and subsequently decomposes the polluting components on the implant surface.

Figure 4 shows SEM morphology of FA nanopwders synthesised at the mentioned conditions above. It can be seen that FA particles attach together and form agglomerated particles of primary FA
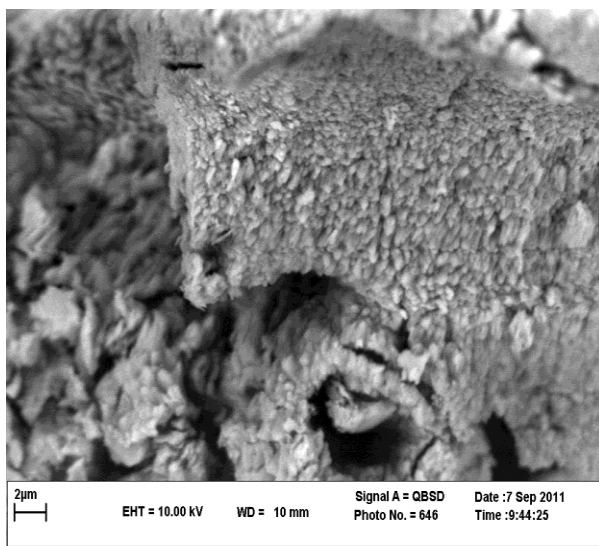
crystallites. It is also clear from Figure 2 that agglomerated particles consist of finer agglomerates that cannot be seen individually in SEM micrograph. Therefore, the size and morphology of fine FA powders were studied by using TEM. Prior to TEM analysis, the FA powders were dispersed ultrasonically in ethanol for 15 min.

Figure 5 shows TEM micrographs of FAp nanopowders. This micrograph confirms that nanosized FA particles were synthesized by sol-gel method. The produced FA nanoparticles have both spherical and rod-like morphology. Nanorod morphology of apatites have gain a lot of attention in recent years. For instance, rod shaped HA shows enhanced protein adsorption because of their charging surface efficiency (Kawachi et al., 2006). HA crystals with rod-like morphology have shown to possess desirable biocompatibility and bioactivity because of better adsorbability, since the underlying Vander Waal's interactions are proportional to the large surface area of the rods (Zandi et al., 2009). Also HA present in human tooth and bone exhibits the form of nano-polycrystalline hexagonal nanorods (Bäuerlein et al., 2007).

3.2. The Effects OF pH

The pH of sols was adjusted from about 12 to about 3. Hydrolysis time and temperature was set at 20 h and 60 ℃, respectively.
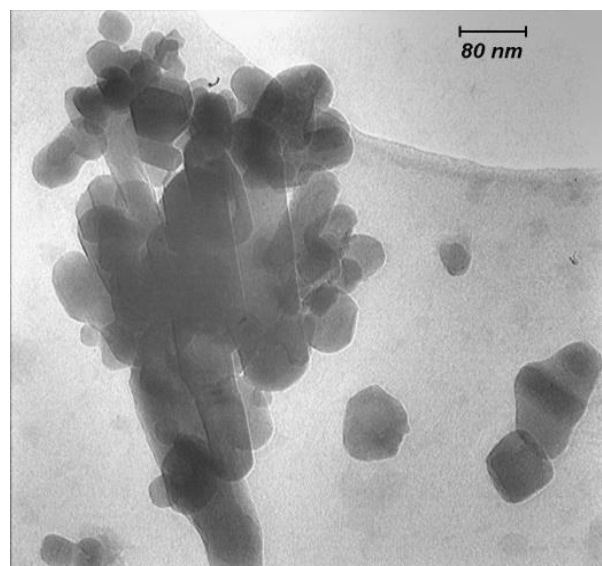

Fig. 4. SEM micrograph of pure FAp synthesised by sol-gel method at pH≈11, hydrolysis time = 20 h and hydrolysis temperature =60 ℃.

Fig. 5. TEM micrograph of pure FAp synthesised by sol-gel method at pH≈11, hydrolysis time = 20h and hydrolysis temperature =60 ℃.

Mixing to gelation was carried at both room temperature and 60 ºC. Figure 6 illustrates the effect of pH on gelation time of FA sols in various mixing temperatures. The results indicated that increasing pH decreases the gelation time of FA sols (Figure 6). The addition of ammonium hydroxide can catalyse the reaction between TEP and calcium nitrate and decrease the gelation time of sols. It can be seen that OH- ions from ammonium hydroxide can attack the hydrolysed triethyl phosphate; this places the triethyl phosphate into a more reactive form which can then react with Ca^{2+} to form the Fluorapatite. With the addition of nitric acid this reaction will still take place, but occurs less completely and much more slowly.

3.3 The Effects of Mixing Temperature

The next parameter investigated was the mixing temperature following addition of the hydrolysed TEP to the calcium nitrate. The mixed solution was mixed at both room temperature and 60 ºC, prior to the gelation. Increasing in mixing temperature of Ca and P sols at each pH significantly decreases the gelation time of sols. Usually conducting a reaction at a higher temperature provides more energy into the system causes more collisions between molecules and increases the reaction rate. At higher temperature of mixing of Ca and P sols, colliding molecules will have the necessary activation energy, resulting in more successful collisions. In fact, increasing the mixing temperature
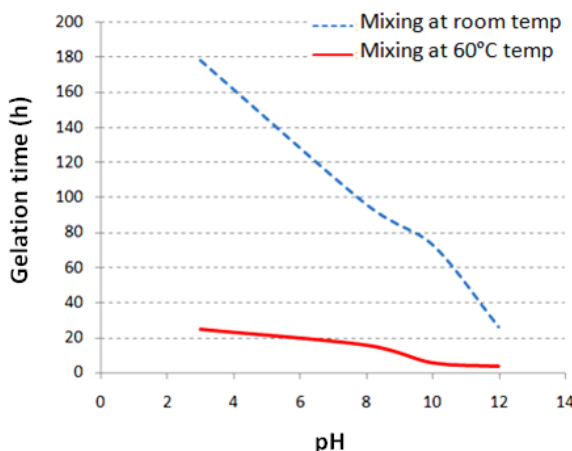
improves the mobility and diffusion speed of the hydrolysed TEP and Ca^{2+} together, and reduces the time of FA formation (Figure 6).

3.4 The Effects of Hydrolysis Time

The effects of hydrolysis time on gelation of FA sol were studied at pH≈11, hydrolysis time of 20 and 48 h at room temperature. Results show that increasing the hydrolysis time of sol from 20 to 48 h, decreases the gelation time from 53 to about 20 h. Figure 7 illustrates a schematic diagram for TEP hydrolysis as time proceeds.

With reference to Figure 7, increasing the hydrolysis time, more OH groups substitutes until hydrolysed TEP forms which can later react with the calcium nitrate to form fluorapatite. Thus, increasing the hydrolysis time of TEP improves the reaction with Ca sol and decreases the gelation time of FA.

4. Conclusions

Fluorapatite nanopowders were prepared by sol-gel technique. The study was focused on the characterization of FA by XRD, FTIR, SEM, TEM and UV-Vis spectroscopy. On synthesis of FAp nanopowders, the effects of sol-gel parameters such as pH, mixing temperature and hydrolysis time were studied. Based on the results obtained, the following conclusions are established:

From XRD and FTIR analyses, pure nano-sized FA powders were synthesized at pH≈11, hydrolysis time = 20 h and hydrolysis temperature = 60 ºC. Mean crystallite size of FA phase after heat treatment at 550 ºC was calculated to be about 70 nm.

The band gaps of pure FA with 70 nm

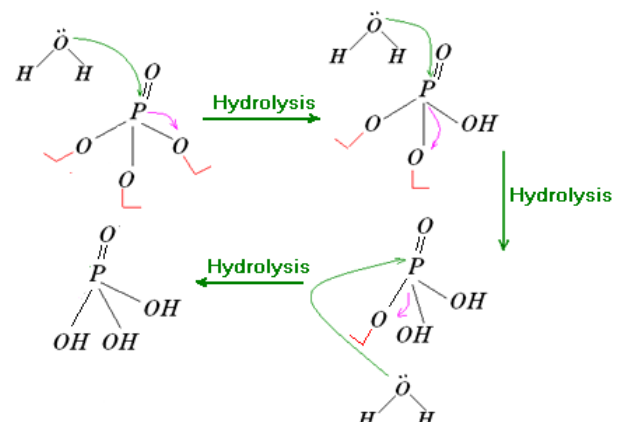**Fig. 6.** Effect of pH on gelation time of FA sols in various mixing temperatures.

Fig. 7. Schematic diagram for TEP hydrolyses.

crystallite-size calculated from Tauc's relation have been found to be about 4.3 eV.

The produced FA nanoparticles have both spherical and rod-like morphology.

Increasing of pH by adding ammonium hydroxide, can improve gelation of FA sols. The OH⁻ ions from ammonium hydroxide attack the hydrolysed TEP and speed up the reaction with Ca^{2+}.

Increasing the time and temperature of hydrolysis of phosphate sols significantly decreased the gelation time of FAp sols.

Mixing of P and Ca sols at 60 ℃, decreases the gelation time of FA sols.

References

1. Kim, H.W., Kong, Y.M., Bae, C.J., Noh, Y.J., Kim, H.E., *Biomater.,* Vol. 25 (2004) pp. 2919–26.

2. Ebrahimi-kahrizsangi, R., Nasiri-Tabrizi, B., Chami, A., *Solid. State. Sci.*, Vol. 12 (2010) pp. 1645-51.

3. Fini, M., Savarino, L., Nicoli Aldini, N., Martini, L., Giavaresi, G., Rizzi, G., Martini, D., Ruggeri, A., Giunti, A., Giardino, R., *Biomaterials*, Vol. 24 (2003) pp. 3183-92.

4. Chen, Y., and Miao, X*., Biomaterials*, Vol. 26 (2005) pp. 1205-10.

5. Block, M. S., Finger, I.M., Fontenot, M.G., Kent, J.N*., Int. J. Oral Maxillofac. Implants.* Vol. 4 (1989) pp. 219–25.

6. Nikcevic, I., Jokanovic, V., Mitric, M., Nedic, Z., Makovec, D., Uskokovic, D., J. *Solid. State. Chem.*, Vol. 177 (2004) pp. 2565–74.

7. Marie, P. J., Hott, M., Metabolism, Vol. 35 (1986) pp. 547-51.

8. Rintoul, L., Wentrup-Byrne, E., Suzuki, S., Grøndahl, L., *J. Mater. Sci- Mater*. M., Vol. 18 (2007) pp.1701–09.

9. Cavalli, M., Gnappi, G. Montenero, A., Bersani, D., Lottici, P.P., Kaciulis, S., Mattogno, G., Fini, M., *J. Mater. Sci.*, Vol. 36 (2001) pp.3253 – 3260.

10. Fa´bia´na, R., Kotsis, I., Zimany, P., Halmos, P., Talanta, Vol. 46 (1998) pp. 1273–77.

11. Fathi, M. H., Mohammadi Zahrani, E*., J. Alloy. Compd*, Vol. 475 (2009) pp. 408–14.

12. Zhang, H. G., Zhu, Q*., J. Mater. Sci.-Mater.* M, Vol. 18 (2007) pp. 1825-9.

13. Wang, J., Chao, Y., Wan, Q., Zhu, Z., Yu, H., *Acta. Biomater.*, Vol. 5 (2009) pp.1798-1807.

14. Brendel, T., Engel, A., Russel, C., (1992), *J. Mater. Sci.- Mater*. M., Vol. 3(1992) pp. 175–9.

15. Lafon, J. P., Champion, E., Bernache-Assollant, D., *J. Eur. Ceram. Soc.*, Vol. 28 (2008) pp. 139-147.

16. Sanosh, K. P., Chu, M.C., Balakrishnan, A., Lee, Y.J., Kim, T.N., Cho, *S.J., Curr. Appl. Phys.*, Vol. 9 (2009) pp. 1459-62.

17. Yadav, R. S., Mishra, P., Mishra, R., Kumar, M., Pandey, A.C., *Ultrason. Sonochem.*, Vol. 17 (2010) pp. 116–22.

18. Mehta, S. K., Chaudhary, S., Kumar, S., Singh, S., *J. Nanopart. Res.*, Vol. 12 (2010), pp. 1697–1709.

19. Rosenman, G., Aronov, D., Oster, L., Haddad, J., Mezinskis, G., Pavlovska, I., Chaikina, M., Karlov, A., *J. Lumin.*, Vol. 122–123 (2007) pp. 936–8.

20. Tsukada, M., Wakamura, M., Yoshida, N., Watanabe, T., *J. Mol. Catal. A.-Chem.*, Vol. 338 (2011) pp. 18–23.

21. Mombelli, A., van Oosten, M.A.C., Schürch, Jr., Lang, E.N.P., *Oral. Microbiol. Immun.*, Vol. 2 (1987) pp. 145–151.

22. Leonhardt, A. Berglundh, T., Ericsson, I., Dahlén, G., Clin. *Oral. Implan. Res.*, Vol. 3 (1992) pp. 112–9.

23. Lindhe, J. Berglundh, T., Ericsson, I., Liljenberg, B., Marinello, C., Clin. *Oral. Implan. Res.*, Vol. 3 (1992) pp. 9–16.

24. Jason Riley, D., Bavastrello, V., Covani, U., Barone, A., Nicolini, C., *Dent. Mater.*, Vol. 21 (2005) pp. 756–60.

25. Kreisler, M., Kohnen, W., Marinello, C., Götz, H., Duschner, H., Jansen, B., d'Hoedt, B., *J. Periodontol*, Vol. 73 (2002) pp. 1292–8.

26. Kreisler, M. Kohnen, W., Marinello, C., Schoof, J., Langnau, E., Jansen, B., d'Hoedt, B., Int. J. *Oral Max. Impl.*, Vol. 18 (2003) pp. 706–11.

27. Dortbudak, O., Haas, R., Bernhart, T., Mailath-Pokorny, G., Clin. *Oral. Implants. Res.,* Vol. 12 (2001) pp. 104–8.

28. Matysik, J., Alia, Bhalu, B., Mohanty, *P., Curr. Sci.*, Vol. 82 (2002) pp. 525–32.

29. Kangwansupamonkon, W., Lauruengtana, V., Surassmu, S., Ruktanonchai, U., *Nanomedicine: Nanotechnology, Biology and Medicine*, Vol. 5 (2009) pp. 240-9.

30. Nonami, T., Taoda, H., Hue, N.T., Watanabe, E., Iseda, K., Tazawa, M., Fukaya, M., *Mater. Res. Bull.*, Vol. 33 (1998) pp. 125-31.

31. Kawachi, G., Sasaki, S., Nakahara, K., Ishida, E. H., Ioku, K., *Key. Eng. Mat*., Vol. 309-311 (2006) pp. 935–8.

32. Zandi, M., Mirzadeh, H., Mayer, C., Urch, H., Eslaminejad, M.B., Bagheri, F., Mivehchi, H., *J. Biomed. Mater. Res*., Vol. 92 (2010) pp. 1244-55.

33. Cuisinier, F., Robinson, C., (In M. Epple, & E. Baeuerlein (Eds.), Handbook of biomineralization: Medical and clinical aspects (2007) pp. 177–82, Weinheim:Wiley-VCH).